Electronic Supplementary Material (ESI) for ChemComm.

Electronic Supporting Information for

A Dipodal Bimane-Ditriazole-Di-Copper Complex Serves as Ultrasensitive Water Sensor

Joy Karmakar, Apurba Pramanik, Vincent Joseph, Vered Marks, Flavio Grynszpan, and Mindy Levine

TABLE OF CONTENTS

MATERIALS AND METHODS

All chemicals, including spectroscopic grade solvents, were purchased from commercial suppliers and used without further purification. All UV/Visible absorption spectra were recorded on a Varian Cary 50 Bio UV-visible spectrophotometer. Fluorescence spectra were recorded on a Varian Cary Eclipse fluorescence spectrophotometer, with emission recorded at a 90^{o} angle relative to the excitation. Slit widths in all cases were 2.5 nm excitation and 2.5 nm emission slit widths, with excitation at 410 nm and a scan speed of 500 nm/minute. ^{1}H NMR spectra were obtained using a Bruker Avance III spectrophotometer operating at 400 MHz. All fluorescence spectra were integrated vs. wavenumber on the X-axis using OriginPro 2021. All curve fitting was done using OriginPro curve fitting options (either linear or non-linear curve fitting, as applicable). All the HR-MS spectra were measured in positive ionization mode using a Waters Micromass Quattro Micro instrument, which was equipped with an electrospray ionization source with Waters 2795 and 996 PDA detectors.

EXPERIMENTAL PROCEDURES

*Experimental Procedure for the Synthesis of Compound **1** (syn-(Me,PhCH$_2$-1N-triazole)bimane)*

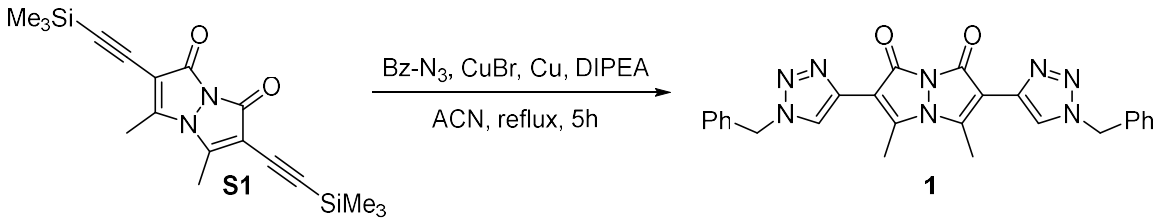

Figure S1. Synthesis of compound **1**

Compound **S1** was prepared following literature-reported procedures.[1-3] Compound **S1** (100 mg, 0.28 mmol, 1.0 eq.) was dissolved in acetonitrile (70 mL) under a nitrogen atmosphere at room temperature, and benzyl azide (74.6 mg, 0.56 mmol, 2.0 eq.) copper bromide (12 mg, 0.05 mmol, 0.18 eq.), copper (0) dust (16 mg, 0.25 mmol, 0.89 eq.) and *N,N*-diisopropylethylamine (0.1 mL, 0.57 mmol, 2.04 eq.) were added. The reaction mixture was refluxed for 5 hours and the solvent was then evaporated under reduced pressure. The crude product was purified using column chromatography (15% ethyl acetate in dichloromethane) to yield compound **1** as a yellow solid (57 mg, 43% yield). ^{1}H NMR ($CDCl_3$, 400MHz): δ 8.17 (s, 1 H), 7.35 (m, 3 H), 7.30 (m, 2 H), 5.55 (s, 2 H), 3.01 (s, 3 H). ^{13}C NMR ($CDCl_3$, 400MHz): δ 157.4, 145.32, 138.25, 134.56, 129.28, 128.97, 128.25, 122.37, 108.11, 54.42, 13.44. LC-MS: m/z calcd. for $C_{26}H_{22}N_8O_2$: 478.19 [MH+]; found: 479.20. HRMS: m/z calcd: 479.1944 [MH+]; found: 479.1972.

Experimental Procedures for UV-Visible and Fluorescence Experiments

Initial Screening of Metals

A stock solution of 1 mM of bimane **1** in acetonitrile was prepared. This solution was then diluted to form 2.5 mL of a 50 μM solution of **1**, and this solution was used for both UV-visible and fluorescence experiments. 1 mM solutions of the following metal salts in acetonitrile were prepared: $Ni(ClO_4)_2$,$CoCl_2$, $Zn(ClO_4)_2.6H_2O$, $SnCl_2.2H_2O$, $HgCl_2$, Cu(II)OTf, $Pd(OAc)_2$, $(Ph_3P)_3RuCl_2$ and $(Ph_3P)_2PtCl_2$. To 2.5 mL of a 50 μM solution of bimane **1** in acetonitrile taken in the cuvette, 100 μL or 200 μL of the various salt solutions (1 mM in acetonitrile) were added, resulting in final concentrations of the salts of 0.038 mM and 0.074 mM, respectively. The full UV-visible spectrum was recorded, followed by measuring the fluorescence emission from excitation at 420 nm, with slit widths of 2.5 nm excitation and 2.5 nm emission. The fluorescence emission spectra were integrated using OriginPro 2021, and the results reported herein represent the average of at least two trials.

Titration Studies

For copper (II) triflate, nickel (II) chlorate, and zinc (II) chlorate hexahydrate, titration studies were conducted. For each of these salts, 2.5 mL of a 25 μM solution of bimane **1** in acetonitrile was taken and 5 μL, 10 μL,20 μL, 30 μL, 40 μL, 50 μL, 100 μL, 200 μL, 300 μL, 400 μL, 500 μL and 1000 μL of a 1mM salt solution in acetonitrile was added. The full UV-visible spectrum was measured after each addition, followed by the fluorescence emission spectrum from excitation at 420 nm. Each experiment was repeated three times, and the results reported herein represent an average of the three trials.

Water Detection Studies

For the detection of water in organic solvents, we prepared a solution of bimane **1** and copper (II) triflate in a variety of water-miscible organic solvents. We then added small amounts of Milli-Q water sequentially to each solution, and measured the UV-visible absorbance and fluorescence emission spectra after each addition. The limits of detection for water in each solvent were calculated using the procedures described on the following page (*vide infra*).

Selectivity Studies

To determine the selectivity of the sensor response to water compared to the response to other analogous analytes, we repeated the water detection studies, but instead of adding small amounts of water to a solution of bimane **1** and copper (II) triflate, we added small amounts of methanol and ethanol, ensuring that the number of moles of each solvent added were equal to the number of moles of water added so that we could do a direct comparison. After each addition, the UV-visible absorbance and fluorescence emission spectra were recorded. We also took photographs and videos of the solutions after addition of the various protic solvents under ambient and 365 nm wavelength excitation.

Benesi-Hildebrand Studies

To determine the binding ratio and binding constant of copper (II) to compound **1**, we performed Benesi-Hildebrand calculations on the results obtained from fluorescence analyses, using Equation S1:[4,5]

$$1/(F\text{-}F_0) = 1/(F_M\text{-}F_0) + 1/(F_M\text{-}F_0) \times 1/[C]^2 \times 1/K \qquad \text{(Eq. S1)}$$

where F_0 = the fluorescence intensity of compound **1** in the absence of Cu(II), F = the fluorescence intensity of compound **1** in presence of Cu(II), F_M = the maximum fluorescence intensity of compound **1** in the presence of Cu(II), [C] = the concentration of the Cu(II) salt, and K = binding constant. Notably, the measured fluorescence intensity at 480 nm showed a linear relationship with $1/[Cu(II)]^2$, which indictes a 1:2 molar ratio of bimane **1** and Cu(II) triflate. The binding constant of the bimane-Cu(II) complex was found to be 5.09×10^8 M^{-1} ($R^2 = 0.99998$) based on the linear Benesi-Hildebrand plot (Fig. SX).

Stern-Volmer Quenching Studies

To determine the quenching constant, we performed Stern-Volmer analyses using the results of the fluorescence experiments in accordance with literature precedent,[6] and plotted the ratio of fluorescence intensities as a function of the concentration of the quencher, in accordance with Equation S2:

$I_0/I = 1 + K_{sv}[Q]$ (Eq. S2)

where [Q] is the quencher concentration, K_{sv} is the Stern-Volmer quenching constant, I_0 = the fluorescence intensity of **1** in the absence of Cu(II), and I = the fluorescence intensity of **1** in the presence of Cu(II). The quenching constant was found to be 1.05 x 10^5 M^{-1} (R^2 = 0.99048), based on the Stern-Volmer plot (Fig. SX).

Experimental Procedure for Quantum Yield Calculations

The fluorescence spectra for calculating the quantum yield of compound **1** in acetonitrile was recorded using a Varian Cary Eclipse fluorescence spectrophotometer equipped with a 10 mm path length quartz cuvette. The excitation slit width was 2.5 nm, the emission slit width was 2.5 nm, and the scan rate was 120 nm/min.

Quantum yields were calculated using the single point relative quantum yield method, using Equation S3:

$$\phi_{F(x)} = (\frac{n_x}{n_s})^2(\frac{A_s}{A_x})(\frac{I_{f(x)}}{I_{f(s)}})\phi_{F(s)} \quad \text{(Eq. S3)}$$

where ϕ_F is the fluorescence quantum yield, A is the absorbance, I_f is the integration of the fluorescence band, and n is the solvent refractive index. The subscripts s and x refer to the standard and unknown sample, respectively. In this work, the fluorescence quantum yield standards were solutions of 1,4-bis(5-phenyloxazol-2-yl)benzene (POPOP) in cyclohexane, with a reported relative quantum yield of 0.97.[7]

*The quantum yield of bimane ditriazole **1** was found to be 0.98 in acetonitrile solution.*

Experimental Procedure for Calculation of the Molar Extinction Coefficient

For the calculation of molar extinction coefficient, we used Beer-Lambert's law, shown in Equation S4:

$A = \varepsilon . c . l$ (Eq. S4)

where A is absorbance, ε is molar extinction coefficient, c is concentration (mol/L) and l is path length (cm). In this calculation, we have taken the absorbance value 0.660 at 415 nm wavelength.

*The molar extinction coefficient of **1** is 1.32 x 10^4 L $M^{-1}cm^{-1}$.*

Experimental Procedures for Limit of Detection Calculations

The limit of detection studies for the detection of water in organic solvents were carried out in four different solvents: acetone, acetonitrile, methanol, and tetrahydrofuran. For these experiments, solutions of bimane **1** (25 μM) and copper (II) triflate (1 mM) were prepared in each of the solvents. For each solvent, 2.5 mL of a 25 μM solution of compound **1** was mixed with 1 mL of a 1 mM solution of copper (II) triflate, and different amounts of Milli-Q water were added: 5 μL, 10 μL, 15 μL, 20 μL and 25 μL. After each addition, the fluorescence emission spectra of the solution were recorded via excitation at 410 nm, and six set of values were taken. This procedure was repeated for each of the four solvents listed above.

After that, a graph of the concentration of water on the X-axis vs. integrated fluorescence emission of the compound **1**-copper (II) complex on the Y-axis was plotted, and the equation for best fit of the data was determined using OriginPro 2021 (either linear or non-linear curve fitting). The limit of detection of the blank, defined as the average of the blank plus three times the standard deviation of the blank, was plugged in as the Y-value for the equation, and the equation was solved for the X-value. This value was reported as the limit of detection of water. Similarly, the limit of quantification of the blank as defined as the average of the blank plus ten times the standard deviation of the blank. When this value was plugged into the best fit equation, the resulting X-value was reported as the limit of quantification of water.

These values were converted from concentration of water (in μM) to percent of water (volume/volume with the organic solvent) in order to enable more direct comparisons with literature-reported values.

Experimental Procedures for ^{1}H NMR Experiments

3.5 mg of bimane **1** were dissolved in 550 μL of DMSO-d_6, and the ^{1}H NMR spectrum was recorded. For the preparation of the complex between compound **1** and copper (II) triflate, copper (II) triflate and compound **1** were dissolved in the same NMR tube and vortexed for 5 minutes, followed by recording of the ^{1}H NMR spectrum. This experiment was done for both a 1:1 molar ratio of compound **1**: copper (II) triflate and a 1:2 molar ratio of compound **1**: copper (II).

Water titration experiments conducted via ^{1}H NMR analysis were then done, using the 1:2 molar ratio of compound **1**: copper (II) triflate solution. To this solution, we added 10 μL of D_2O in the NMR tube and vortexed for five minutes, followed by re-recording of the ^{1}H NMR spectrum. We subsequently added additional D_2O for total volumes of 20 μL, 30 μL, 50 μL, and 150 μL, and after each addition, we vortexed the ^{1}H NMR tube and measured the spectrum.

Two-dimensional NMR experiments were conducted in order to determine key correlations and to identify the bonding of copper to the starting material. These experiments were done by dissolving bimane **1** in DMSO-d_6, followed by filtration of the compound that did not dissolve (3.5 mg of compound **1** in 550 μL of DMSO-$d_6$prior to dissolution. The following two-dimensional experiments were then performed: ^{1}H/^{13}C HMQC and HMBC; and ^{1}H/^{15}N HMBC.

Experimental Procedures for FTIR Experiments

1.15 mg of compound **1** were ground by hand with a mortar and pestle for approximately 2-3 minutes. The resulting solid-state mixture was mixed with a KBr salt and pellets from the solid-state mixture were formed using a hydraulic pressure apparatus. To measure the solid-state FTIR spectra of the samples, first a background correction scan was conducted using a KBr pellet (without the sample). Following that, pellets made with the sample were placed in the FTIR spectrometer and the spectra were acquired. We then added 1.65 mg Cu (II) triflate (1:2 molar ratio of compound **1** to the copper (II) triflate) to the sample, made pellets, and recorded FTIR spectrum. We followed the same procedure to prepare KBr pellets of copper (II) triflate alone, and recorded the FTIR spectrum of these pellets. All data were saved as ASCII files and plotted using OriginPro 2021 software.

SUMMARY TABLES

Summary Tables of Fluorescence Data from Metal Complexation Experiments

Table S1. Summary of changes to the fluorescence emission spectrum of compound **1** with the addition of metal (II) salts[a]

	Normalized integration at low metal ion concentration	Normalized integration at high metal ion concentration
bimane	0.98 ± 0.1	0.98 ± 0.1
Ru	0.97 ± 0.1	0.96 ± 0.1
Pd	0.96 ± 0.1	0.93 ± 0.1
Pt	0.97 ± 0.1	0.97 ± 0.1
Cu	0.56 ± 0.1	0.24 ± 0.1
Zn	0.86 ± 0.1	0.77 ± 0.1
Ni	0.85 ± 0.1	0.72 ± 0.1
Co	0.96 ± 0.1	0.94 ± 0.1
Sn	1.00 ± 0.1	0.98 ± 0.1
Hg	0.99 ± 0.1	0.97 ± 0.1

[a] [**1**] = 50 μM; low metal ion concentration = 0.038 mM; high metal ion concentration = 0.074 mM. These measurements were conducted as a preliminary screening of metal-induced effects and represent the results of a single measurement. Errors shown represent the error of the instrument measurements.

Table S2. Summary of the changes to the fluorescence emission spectrum of compound **1** with the addition of increasing concentrations of copper, zinc, and nickel (II) salts[a]

[M(II)] (mM)	Normalized integration in the presence of copper (II)	Normalized integration in the presence of zinc (II)	Normalized integration in the presence of nickel (II)
0	1.00 ± 0.1	1.00 ± 0.1	1.00 ± 0.1
0.038	0.57 ± 0.1	0.88 ± 0.1	0.87 ± 0.1
0.074	0.25 ± 0.1	0.79 ± 0.1	0.74 ± 0.1
0.107	0.14 ± 0.1	0.72 ± 0.1	0.62 ± 0.1
0.138	0.09 ± 0.1	0.67 ± 0.1	0.56 ± 0.1
0.167	0.07 ± 0.1	0.63 ± 0.1	0.50 ± 0.1
0.286	0.03 ± 0.1	0.49 ± 0.1	0.33 ± 0.1

[a] [**1**] = 50 μM. Integration was done between 410 and 700 nm, using OriginPro 2021 software. These measurements were conducted as a preliminary screening of metal-induced effects and represent the results of a single measurement. Errors shown represent the error of the instrument measurements.

Table S3. Summary of the changes to the fluorescence emission spectrum of compound **1** with the addition of increasing concentrations of copper (II) triflate[a]

[Cu] (mM)	Normalized absorbance integration[b]	Normalized fluorescence integration[c]

0	0.17 ± 0.0001	1.00 ± 0.003
0.004	0.21 ± 0.0003	0.97 ± 0.002
0.008	0.23 ± 0.0001	0.93 ± 0.002
0.012	0.24 ± 0.0001	0.89 ± 0.001
0.016	0.26 ± 0.0002	0.85 ± 0.001
0.02	0.28 ± 0.0001	0.81 ± 0.001
0.038	0.37 ± 0.0001	0.64 ± 0.000
0.074	0.55 ± 0.0003	0.42 ± 0.000
0.107	0.71 ± 0.0007	0.29 ± 0.000
0.138	0.86 ± 0.0020	0.21 ± 0.000
0.167	1.00 ± 0.0044	0.15 ± 0.000
0.286	*d*	0.05 ± 0.001

[a] [**1**] = 50 μM; [Cu(II)] = 0 mM-0.286 mM; all results represent the average of at least three trials

[b] The UV-visible absorbance spectra were integrated from 210-700 nm using OriginPro 2021 software

[c] The fluorescence emission spectra were integrated from 430-700 nm using OriginPro 2021 software, with slit widths of 2.5 nm excitation and 2.5 nm emission.

[d] The absorption spectrum at this concentration of copper maxed out the detector; as a result; accurate integration of the absorption spectrum could not be obtained.

Summary Tables of UV-Visible and Fluorescence Data from Water Quenching Experiments[a]

Table S4. Summary of the changes to the UV-visible absorbance and fluorescence emission spectra of compound **1** with the addition of increasing concentrations of Milli-Q water[a]

[H_2O] (mM)	Absorbance integration	Fluorescence integration
0.00	*b*	0.14 ± 0.000
1.58	*b*	0.18 ± 0.000
3.16	*b*	0.27 ± 0.001
4.74	*b*	0.35 ± 0.001
6.32	*b*	0.42 ± 0.001
7.90	*b*	0.48 ± 0.002
15.80	*b*	0.67 ± 0.002
31.60	*b*	0.90 ± 0.001
47.40	0.95 ± 0.050	1.00 ± 0.001
63.20	0.76 ± 0.014	1.00 ± 0.001
79.00	0.62 ± 0.004	0.97 ± 0.001
158.00	0.30 ± 0.001	0.82 ± 0.002

[a] All integration values were normalized to 1.0 for the maximum integration value. Absorbance spectra were integrated between 220 and 700 nm; fluorescence spectra were integrated between 430 and 700 nm. [**1**] = 25 μM; [Cu(II)] = 1 mM; slit widths = 2.5 nm excitation and 2.5 nm emission.

[b] Absorbance spectra at these concentrations maxed out the detector, and so accurate integration could not be determined.

Summary Tables of Fluorescence Data from Selectivity Experiments

Table S5. Percent recovery of the initial fluorescence of bimane **1** upon the addition of methanol, ethanol, or water[a]

Moles solvent[b]	Ethanol	Methanol	Water
0.0001	2.2 %	2.2 %	3.2 %
0.0005	2.6 %	2.7 %	5.7 %
0.001	3.2 %	3.0 %	9.8 %
0.005	6.5 %	9.5 %	46.9 %
0.01	10.2 %	17.4 %	59.3 %

[a] Percent recovery is defined according to the following equation:

$I_{solvent} / I_{blank} * 100$ %,

where $I_{solvent}$ represents the integration of the fluorescence emission spectra in the presence of a given amount of solvent, and I_{blank} represents the integration of the initial fluorescence emission spectrum of bimane **1** before any additions.

[b] "Moles solvent" refers to the moles of solvent added to a 2.5 mL solution of bimane **1** and copper (II) triflate in acetonitrile

Summary Tables for Limit of Detection Experiments

Table S6. Limits of detection and quantification of trace amounts of water using a copper (II)-bimane complex[a]

Solvent	LOD (v/v)	LOQ (v/v)	Equation	R^2
Acetone	$(1.29 \pm 0.07) \times 10^{-3}$	$(6.820 \pm 0.007) \times 10^{-4}$	y = 407064x + 63244	0.9813
Acetonitrile	$(4.594 \pm 0.358) \times 10^{-3}$	$(4.343 \pm 0.358) \times 10^{-3}$	y = 124179x + 57345	0.9812
Tetrahydrofuran	$(0.786 \pm 0.0035) * 10^{-3}$	$(1.496 \pm 0.0035) * 10^{-3}$	*b*	0.97839

a Limits of detection and quantification were calculated following literature-reported procedures after the data was fit to a linear or non-linear equation. Results reported herein represent an average of at least three trials.

b The data was fit to a non-linear equation with the following parameters: y = A1*exp(-x/t1) + A2*exp(-x/t2) + y0; A1 = -866099; t1 = 0.32685; A2 = -880509; t2 = 0.32682; y0 = 2223175; R^2 = 0.97839

Table S7. A comparison of the results reported herein to literature-reported luminescent water sensors

Compound	**Solvent**	**LOD (v/v %)**	**Reference**
$Eu(TTA)_3$phen Complex	EtOH	0.002	*8*
$Eu(DAF)_2(NO_3)_3$	MeCN	0.030	*9*
Hydrazone-acetate Complex	MeCN	0.037	*10*
	THF	0.071	
N-allyl-4-morpholinyl-1,8-naphthalimide	MeCN	0.006	*11*
N-amino-4-(2-hydroxyethylamino)-1,8-naphthalimide	Dioxane	0.019	*12*
	MeCN	0.038	
	EtOH	0.060	
4-(1-piperidyl)-N-(2-pyrimidinyl)-1,8-naphthalimide	Acetone	0.016	*13*
	THF	0.020	
Copper-dansyl-bipyridine complex	Acetone	0.003	*14*
Copper-coumarin complex	MeOH	0.0525	*15*
Bimane diboronate ester	MeCN	0.57	*16*
	THF	5.74	
	DMF	0.17	
	DMSO	0.018	
	Acetone	0.76	
Bimane-Cu Complex	Acetone	0.0012	our work
	MeCN	0.0045	
	THF	0.0007	

Summary Tables of ^1H NMR Titration Experiments

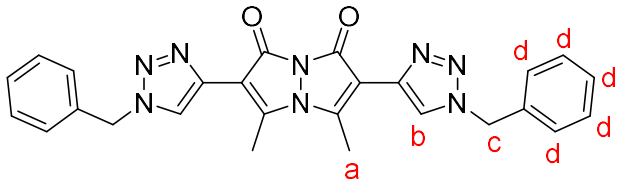

Table S8. Chemical shifts for the proton signals of compound **1** when mixed in a 1:1 and 1:2 stoichiometric ratio with copper (II) triflate

Proton	Proton signals of **1**	Proton signals of **1** in a 1:1 ratio with Cu(II)	Proton signals of **1** in a 1:2 ratio with Cu(II)	Δδ (ppm) from the 1:1 ratio	Δδ (ppm) from the 1:2 ratio
H_a	2.928	2.918	2.879	-0.010	-0.049
H_b	8.481	8.484	8.498	0.003	0.017
H_c	5.686	5.669	5.648	-0.017	-0.038
H_d	7.359	7.349	7.316	-0.010	-0.043

[a] All spectra were acquired on a 400 MHz NMR; solvent: DMSO-d_6; temperature: 300 K; sample prepared by adding 3.5 mg of compound **1** to 550 µL of DMSO-d_6, followed by filtering of the solution prior to spectral acquisition

Table S9, Chemical shifts for the proton signals of compound **1** in a 1:2 complex with copper (II) triflate upon the addition of increasing amounts of D_2O

Proton	Proton signals of **1**	Δδ (ppm) with 10 µL D_2O	Δδ (ppm) with 20 µL D_2O	Δδ (ppm) with 30 µL D_2O	Δδ (ppm) with 50 µL D_2O	Δδ (ppm) with 150 µL D_2O
H_a	2.928	-0.058	-0.067	-0.076	-0.092	-0.168
H_b	8.481	0.013	0.015	0.019	0.026	0.216
H_c	5.686	-0.046	-0.052	-0.057	-0.068	-0.086
H_d	7.359	-0.046	-0.049	-0.052	-0.056	-0.071

[a] All spectra were acquired on a 400 MHz NMR; solvent: DMSO-$d_6$temperature: 300 K; sample prepared by adding 3.5 mg of compound **1** to 550 µL of DMSO-d_6*6*, followed by filtering of the solution prior to spectral acquisition

SUMMARY FIGURES

*Summary Figures for the Synthesis of Compound **1***

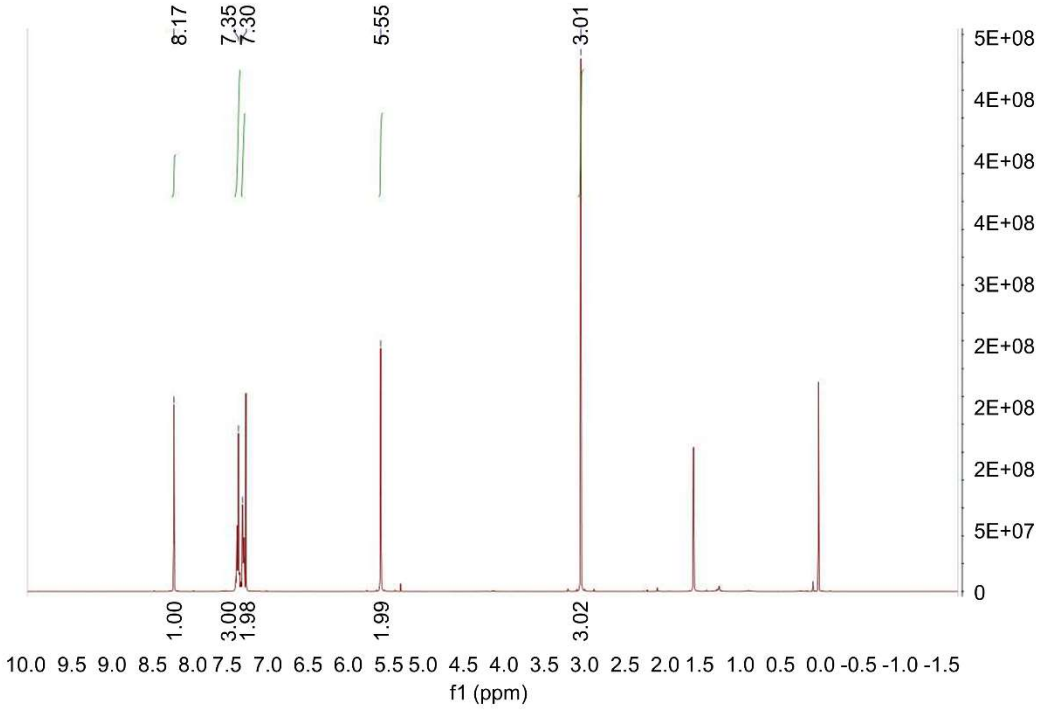

Figure S2. ^{1}H NMR of compound **1** in $CDCl_3$

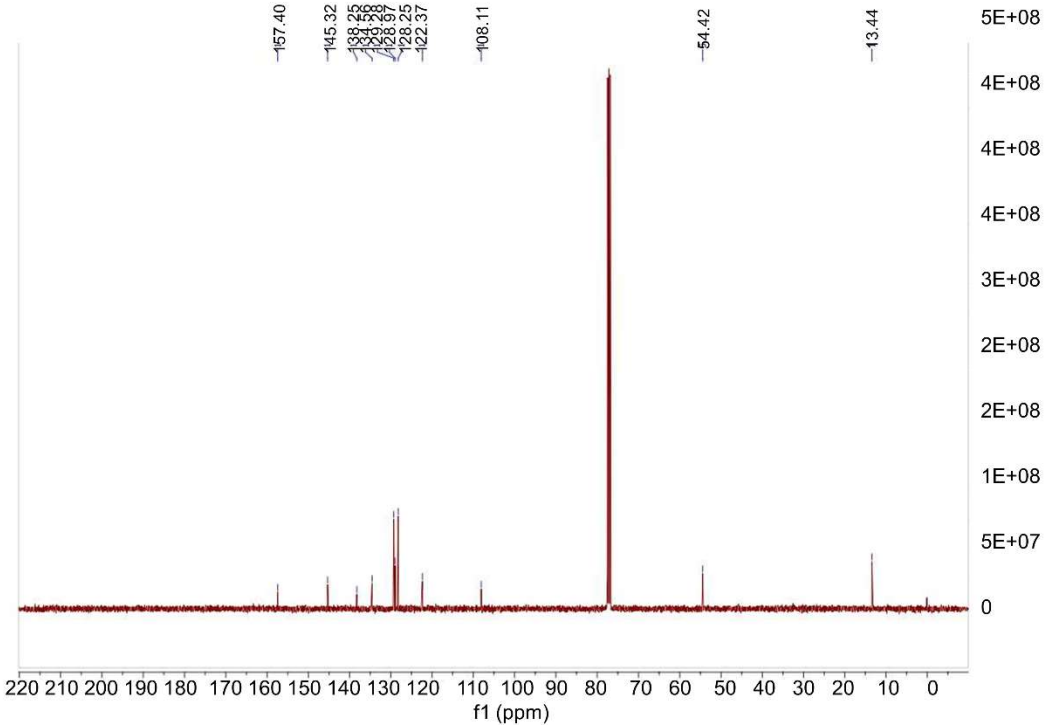

Figure S3. ^{13}C NMR of compound **1** in $CDCl_3$

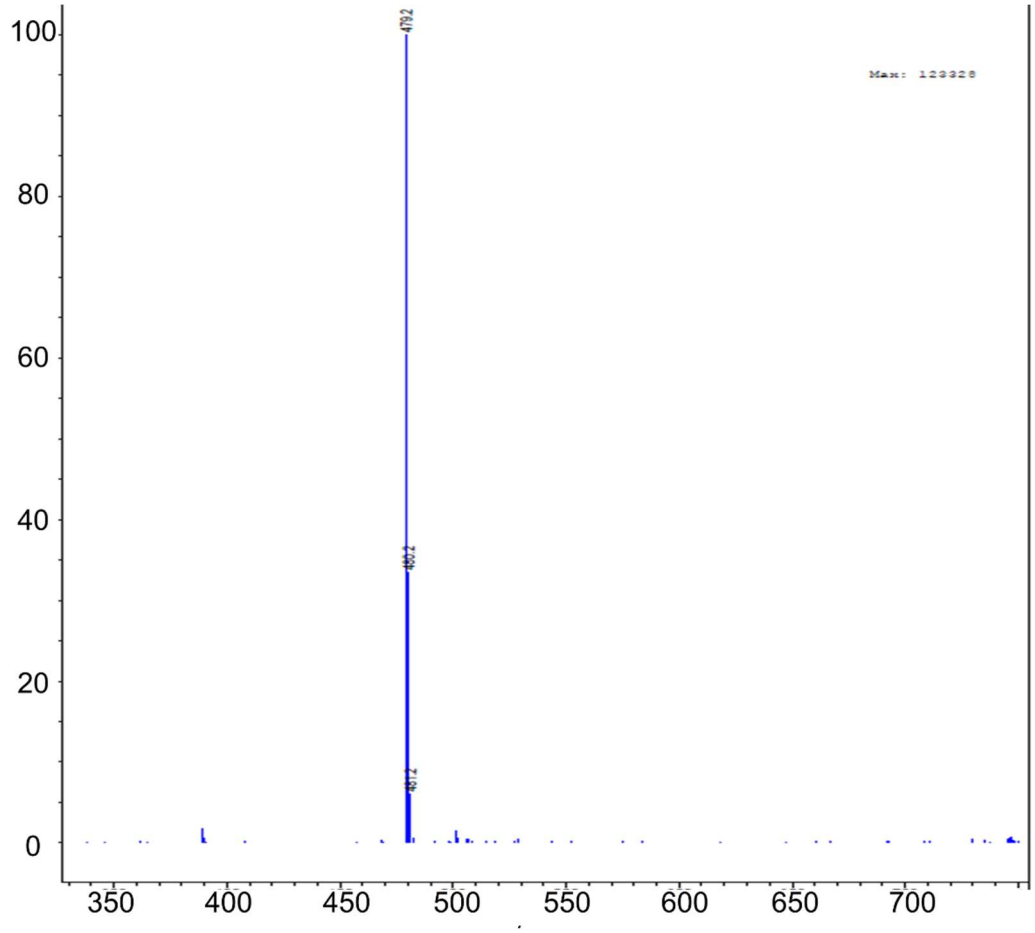

Figure S4. Mass spectrum of compound **1**

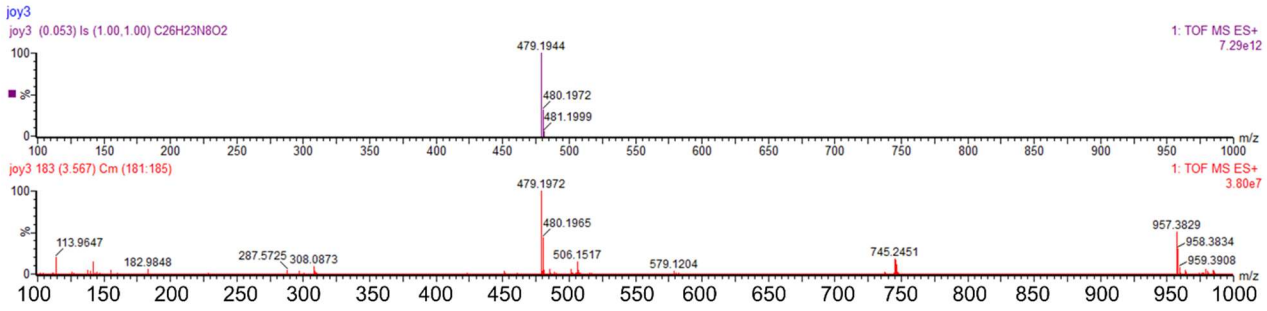

Figure S5. High resolution mass spectrum of compound **1** (top spectrum: simulated isotopic model; bottom spectrum: experimentally obtained results)

Summary Figures for Metal Ion-Induced Changes in Bimane UV-Visible Absorption Spectrum

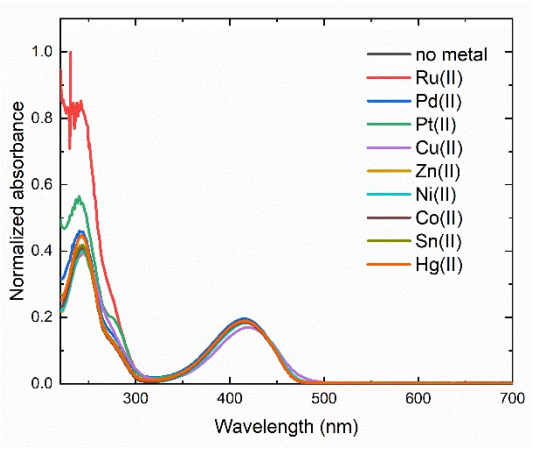

Figure S6. Normalized UV-visible absorbance spectra of bimane **1** in the presence of 0.038 mM metal (II) salts

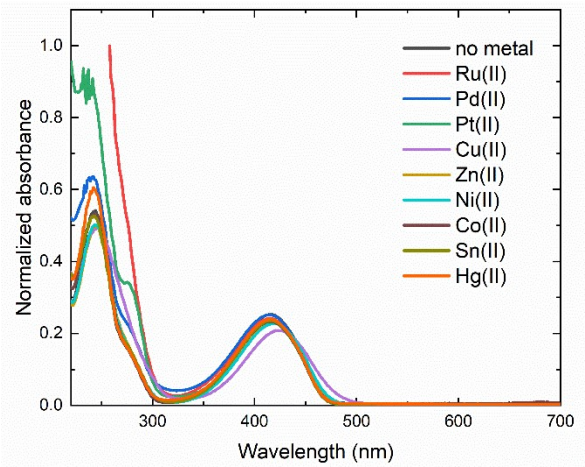

Figure S7. Normalized UV-visible absorbance spectra of bimane **1** in the presence of 0.074 mM metal (II) salts

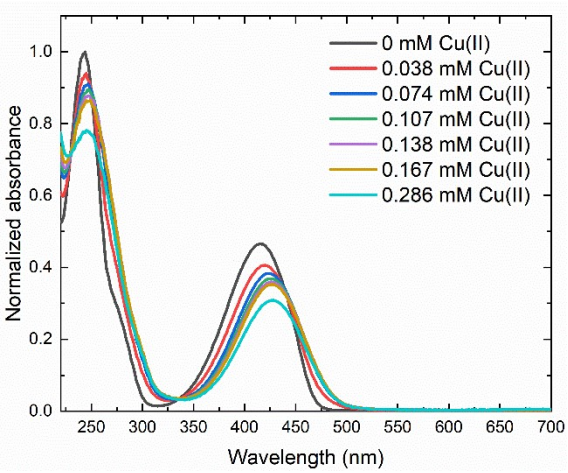

Figure S8. Normalized UV-visible absorbance spectra of bimane **1** in the presence of increasing concentrations of copper (II) triflate

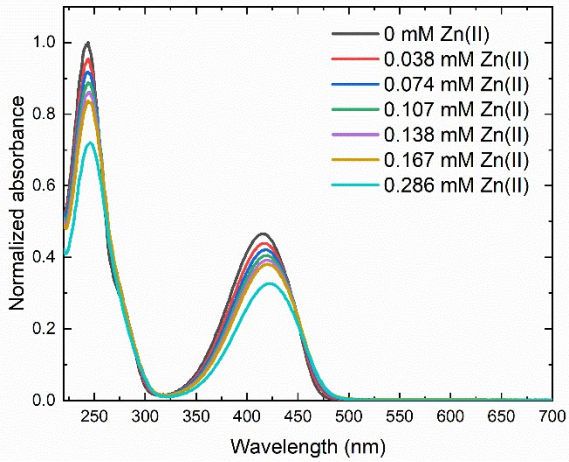

Figure S9. Normalized UV-visible absorbance spectra of bimane **1** in the presence of increasing concentrations of zinc (II) chlorate

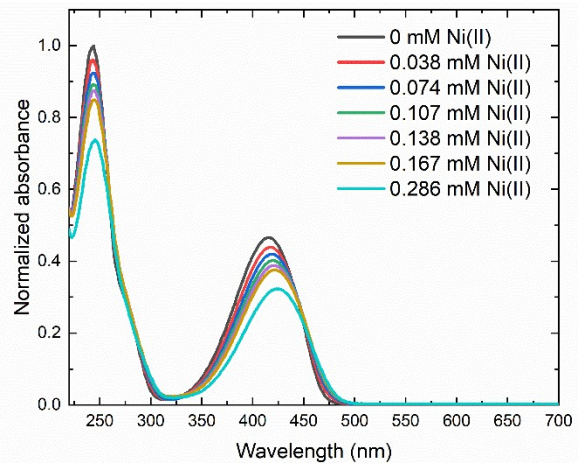

Figure S10. Normalized UV-visible absorbance spectra of bimane **1** in the presence of increasing concentrations of nickel (II) chlorate

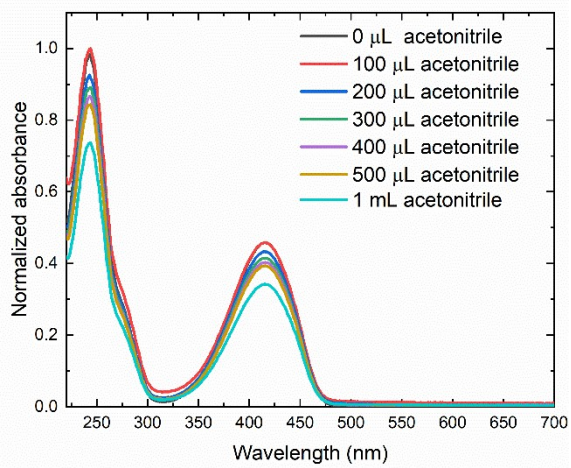

Figure S11. Normalized UV-visible absorbance spectra of bimane **1** in the presence of increasing amounts of acetonitrile

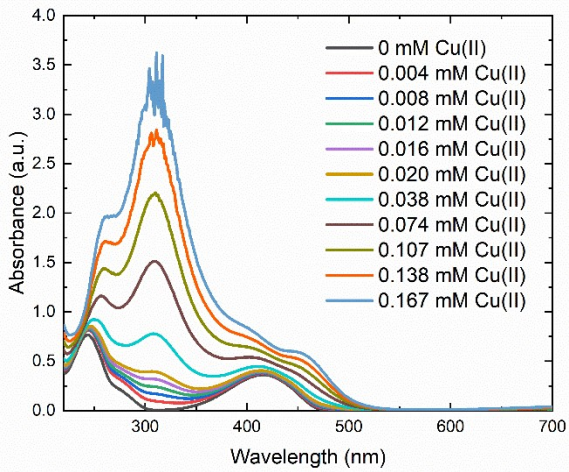

Figure S12. Normalized UV-visible absorbance spectra of bimane **1** in the presence of increasing amounts of copper (II) triflate

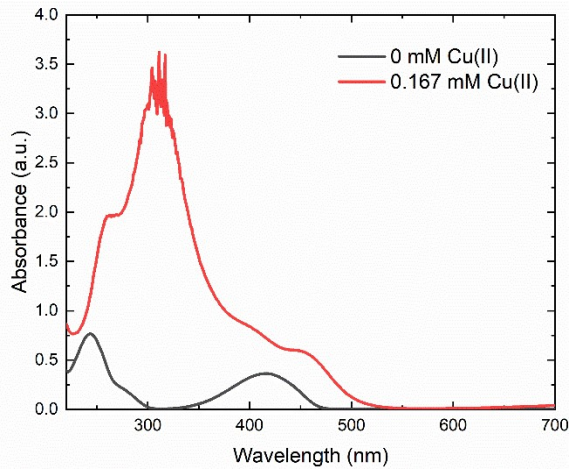

Figure S13. Summary of the normalized UV-visible absorbance spectra of bimane **1** in the presence of increasing amounts of copper (II) triflate

Summary Figures for Metal Ion-Induced Changes in Bimane Fluorescence Emission Spectrum

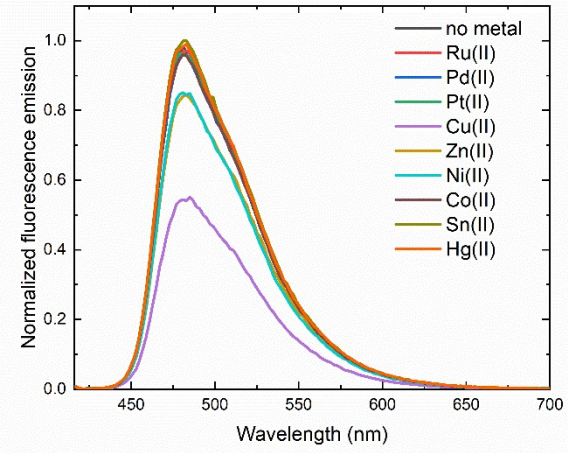

Figure S14. Normalized fluorescence emission spectra of bimane **1** in the presence of 0.038 mM metal (II) salts

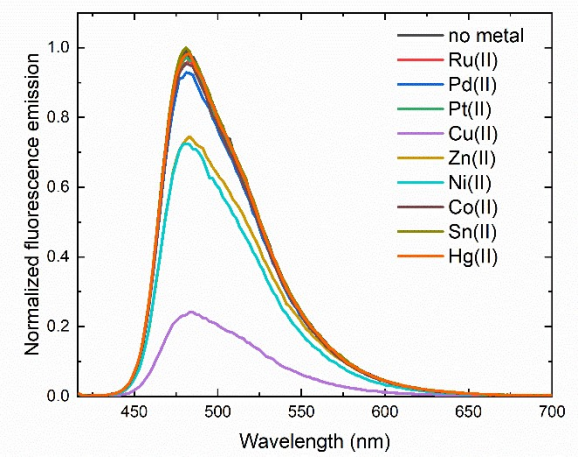

Figure S15. Normalized fluorescence emission spectra of bimane **1** in the presence of 0.074 mM metal (II) salts

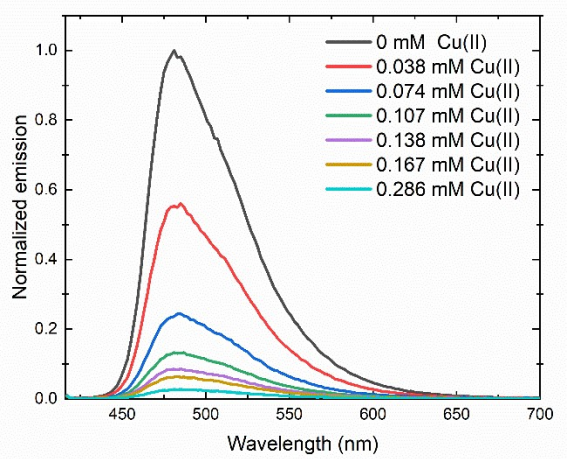

Figure S16. Normalized fluorescence emission spectra of bimane **1** in the presence of increasing concentrations of copper (II) triflate

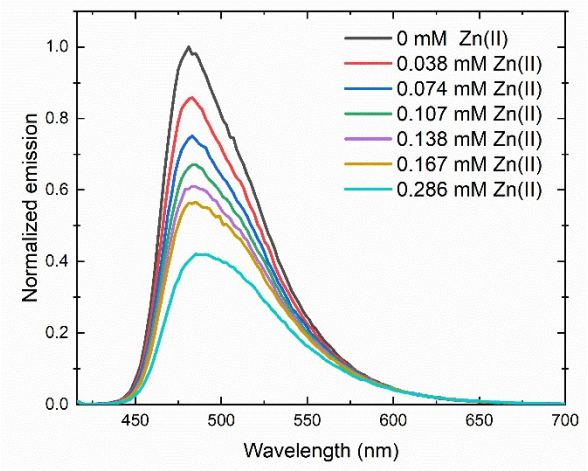

Figure S17. Normalized fluorescence emission spectra of bimane **1** in the presence of increasing concentrations of zinc (II) chlorate

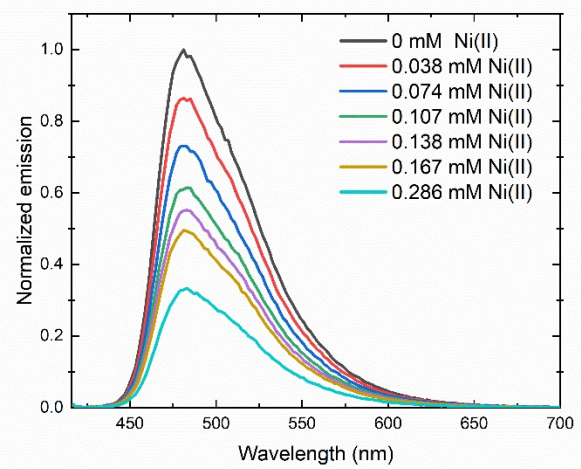

Figure S18. Normalized fluorescence emission spectra of bimane **1** in the presence of increasing concentrations of nickel (II) chlorate

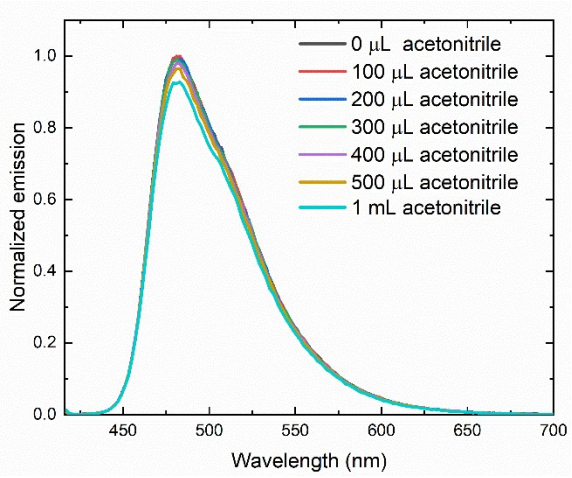

Figure S19. Normalized fluorescence emission spectra of bimane **1** in the presence of increasing amounts of acetonitrile

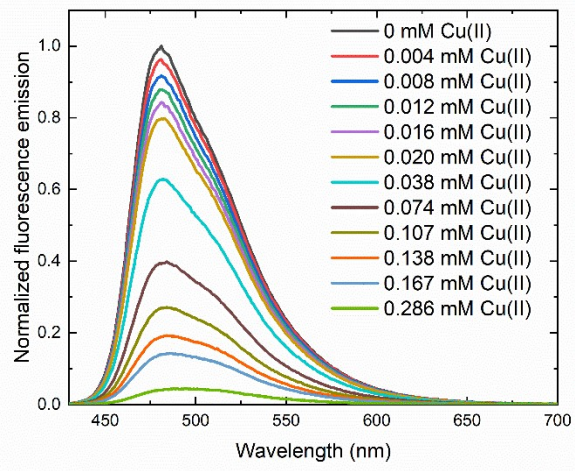

Figure S20. Normalized fluorescence emission spectra of bimane **1** in the presence of increasing amounts of copper (II) triflate

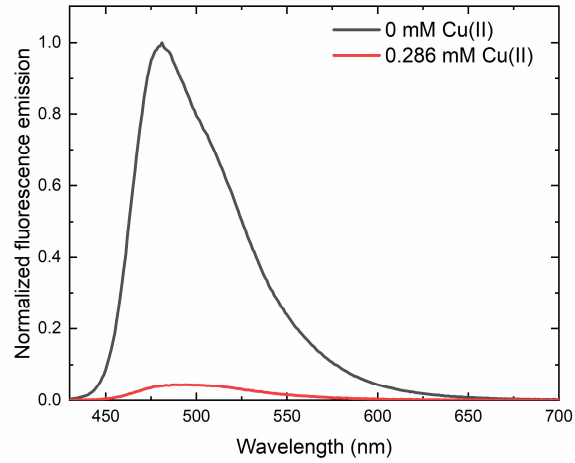

Figure S21. Summary of the normalized fluorescence emission spectra of bimane **1** in the presence of increasing amounts of copper (II) triflate

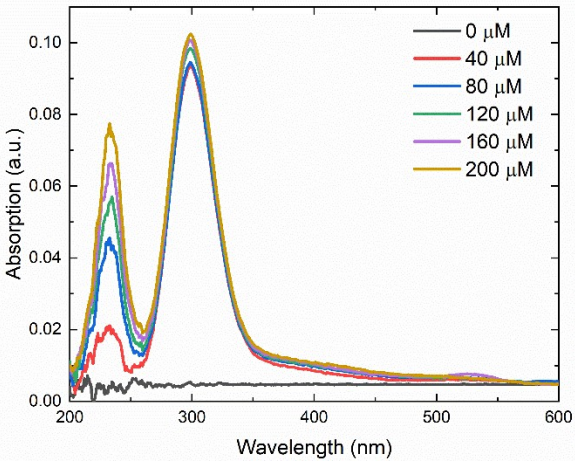

Figure S22. UV-visible absorbance spectra of copper (II) triflate in acetonitrile at different concentrations

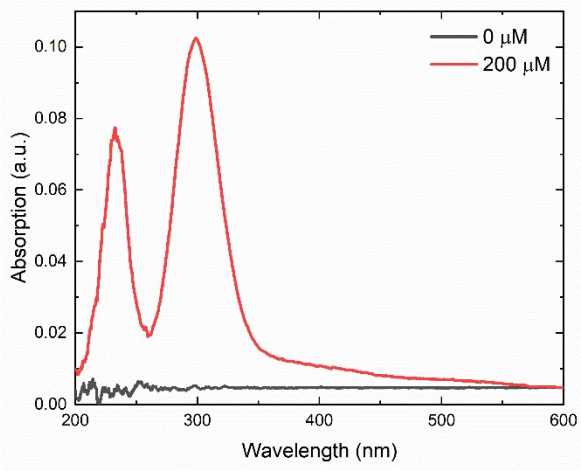

Figure S23. Summary of the changes in the UV-visible absorbance spectra of copper (II) triflate with increasing concentrations of copper (II) triflate

Summary Figures of UV-Visible Absorption Data from Water Quenching Experiments

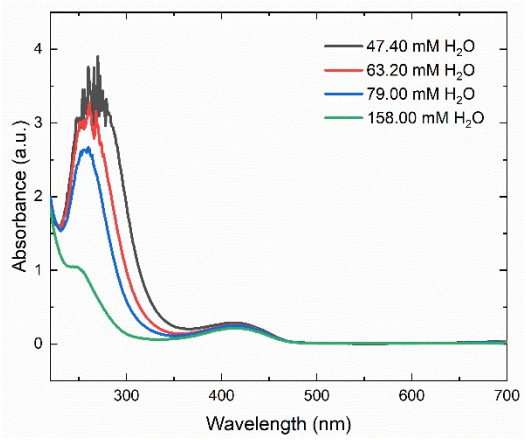

Figure S24. UV-visible absorbance of a copper (II)-bimane **1** complex in the presence of increasing concentrations of water

Summary Figures of Fluorescence Emission Data from Water Quenching Experiments

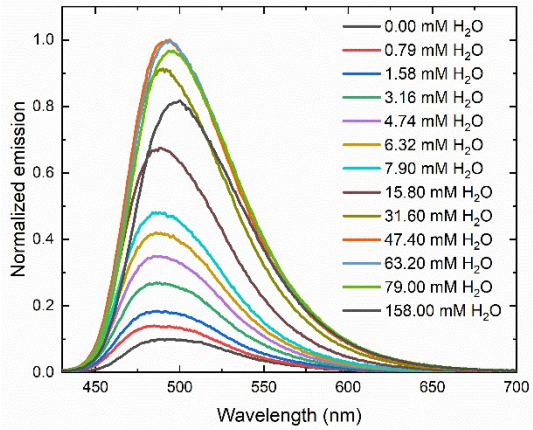

Figure S25. Fluorescence emission of a copper (II)-bimane **1** complex in the presence of increasing concentrations of water

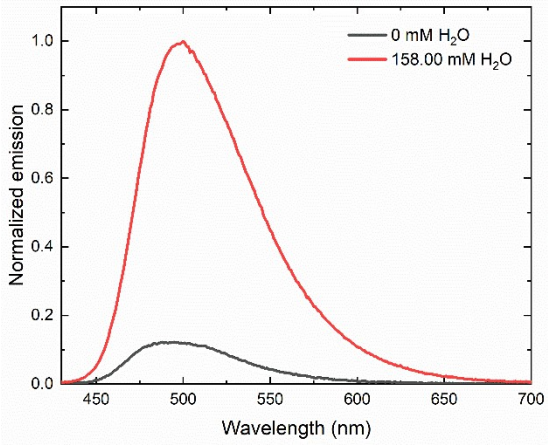

Figure S26. Summary of the fluorescence emission changes of a copper (II)-bimane **1** complex in the presence of increasing concentrations of water

ML

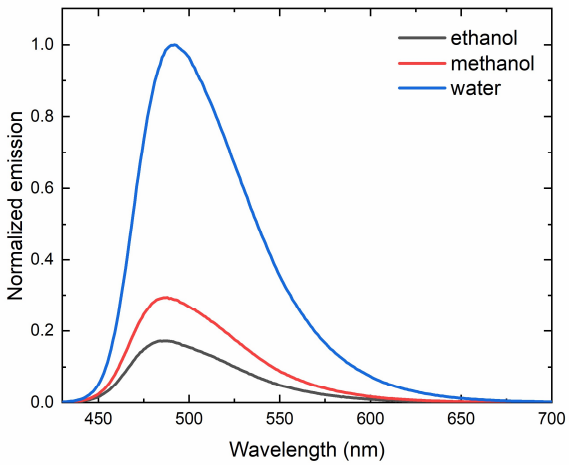

Figure S27. Comparison of the fluorescence emission spectra of a compound **1**- copper (II) triflate complex upon the addition of 500 µL (12.5% v/v) of ethanol (grey line), methanol (red line), and water (blue line).

Summary Photographs from Water Quenching and Selectivity Experiments

Figure S28. Photograph under long-wave TLC lamp irradiation (365 nm) of a solution of compound **1** mixed with copper (II) triflate (1:2 molar ratio) after the addition of 0.01 moles of solvent: water (left-most vial), methanol (middle vial) and ethanol (right-most vial); ([**1**] = 25 µM)

Summary Figures for Benesi-Hildebrand and Stern-Volmer Plots

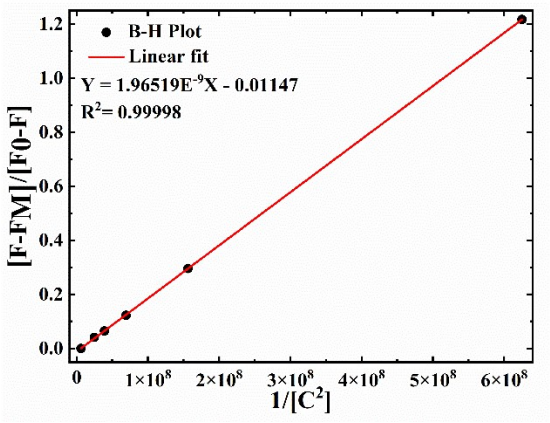

Figure S29. Benesi-Hildebrand plot for the interaction of bimane **1** with copper (II), with the best linear fit of the data showing a 1:2 bimane: copper stoichiometry. Binding constant from this plot: 5.09 x 10^8 M^{-1}

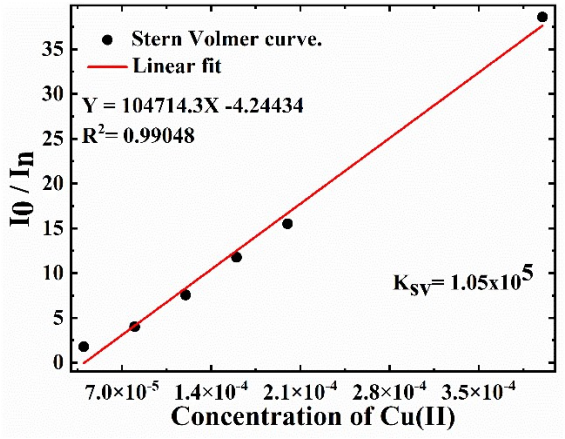

Figure S30. Stern-Volmer plot for the interaction of a bimane **1** with copper (II) triflate, with the best linear fit of the data showing a quenching constant (K_{SV}) of 1.05 x 10^5 M^{-1}

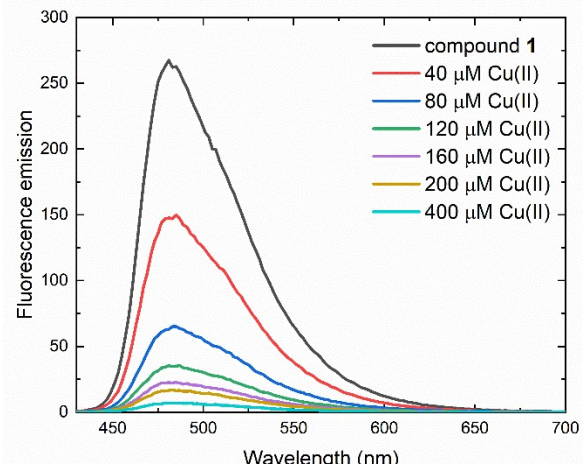

Figure S31. Summary figure of fluorescence quenching of compound **1** induced by sequential additions of copper (II) triflate

Summary Figures for Limit of Detection Calculations

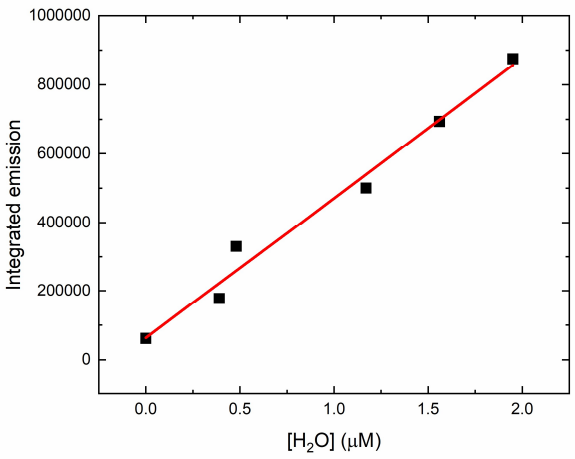

Figure S32. Summary figure for limit of detection calculations of water in acetone using a bimane **1**- copper complex

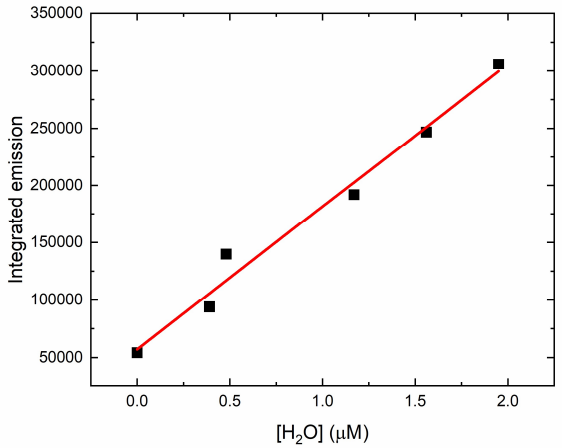

Figure S33. Summary figure for limit of detection calculations of water in acetonitrile using a bimane **1**- copper complex

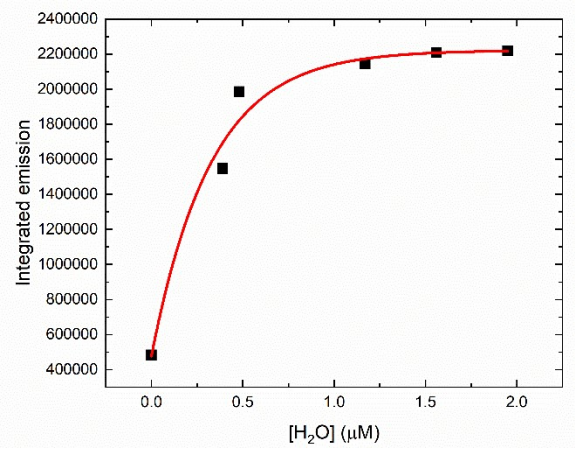

Figure S34. Summary figure for limit of detection calculations of water in tetrahydrofuran (THF) using a bimane **1**- copper complex

Summary Figures for ^1H NMR Titrations

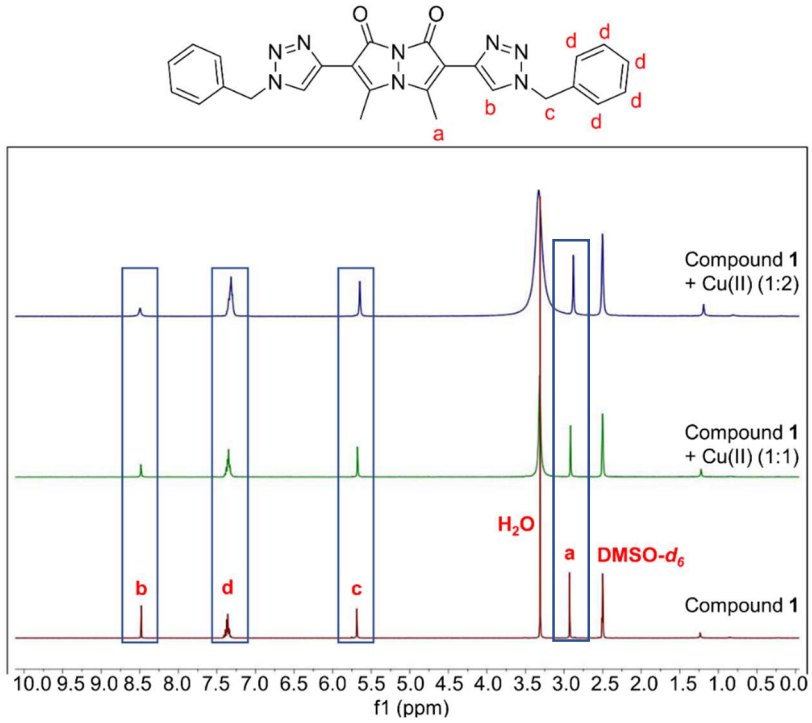

Figure S35. ^1H NMR spectra of compound **1** (bottom spectrum) in the presence of one equivalent (middle spectrum) and two equivalents (upper spectrum) of copper (II) triflate

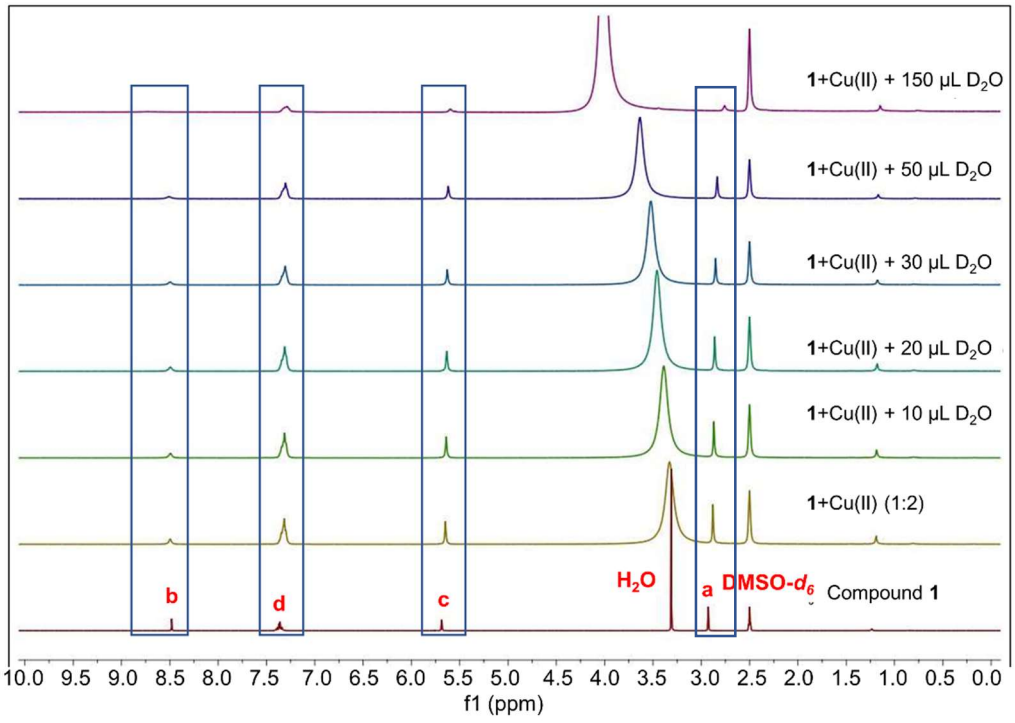

Figure S36. ^1H NMR spectra of compound **1** in a 1:2 complex with copper (II) triflate upon the addition of increasing amounts of D_2O (0-150 µL)

Summary Figures for Two-Dimensional NMR Experiments

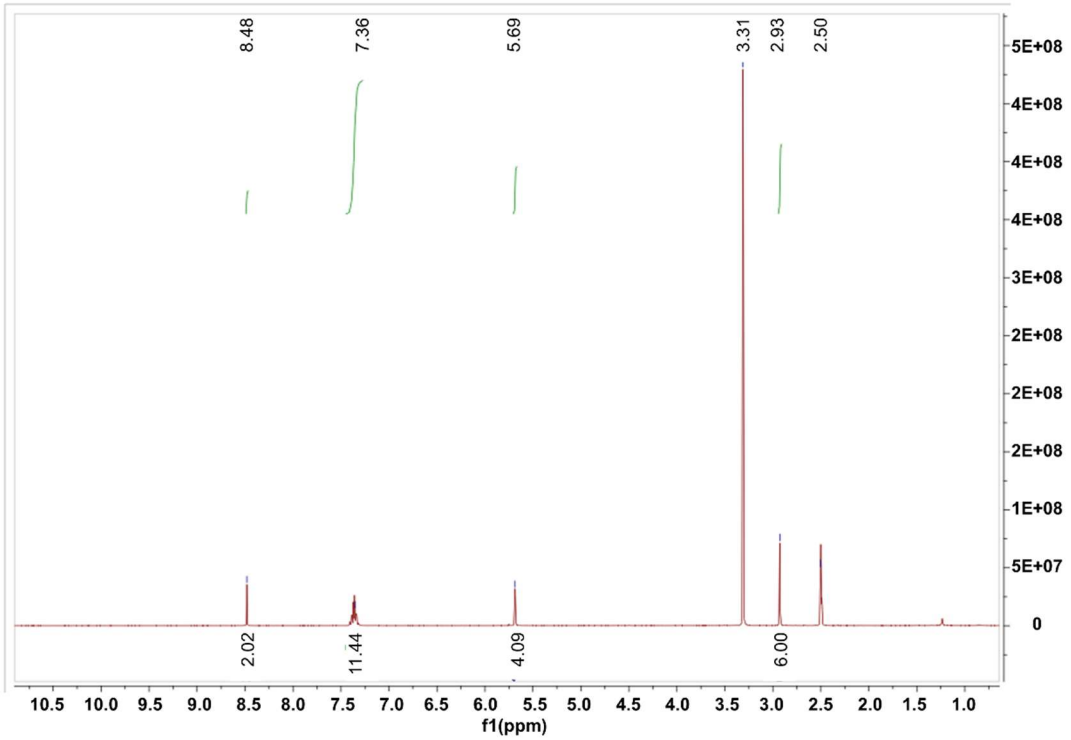

Figure S37. ^{1}H NMR spectra in DMSO-d$_6$ solvent of bimane ditriazole **1** at 300 K

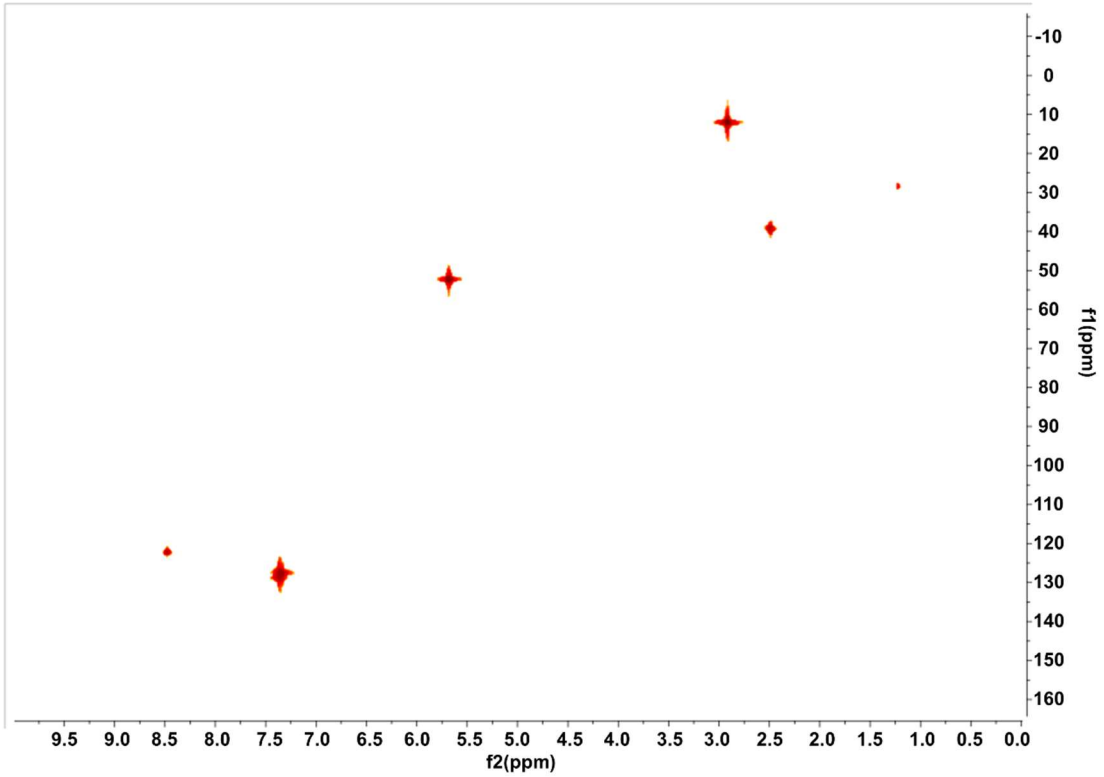

Figure S38. HMQC ^{13}C-^{1}H correlation in DMSO-d$_6$ solvent of bimane ditriazole 1 at 300 K

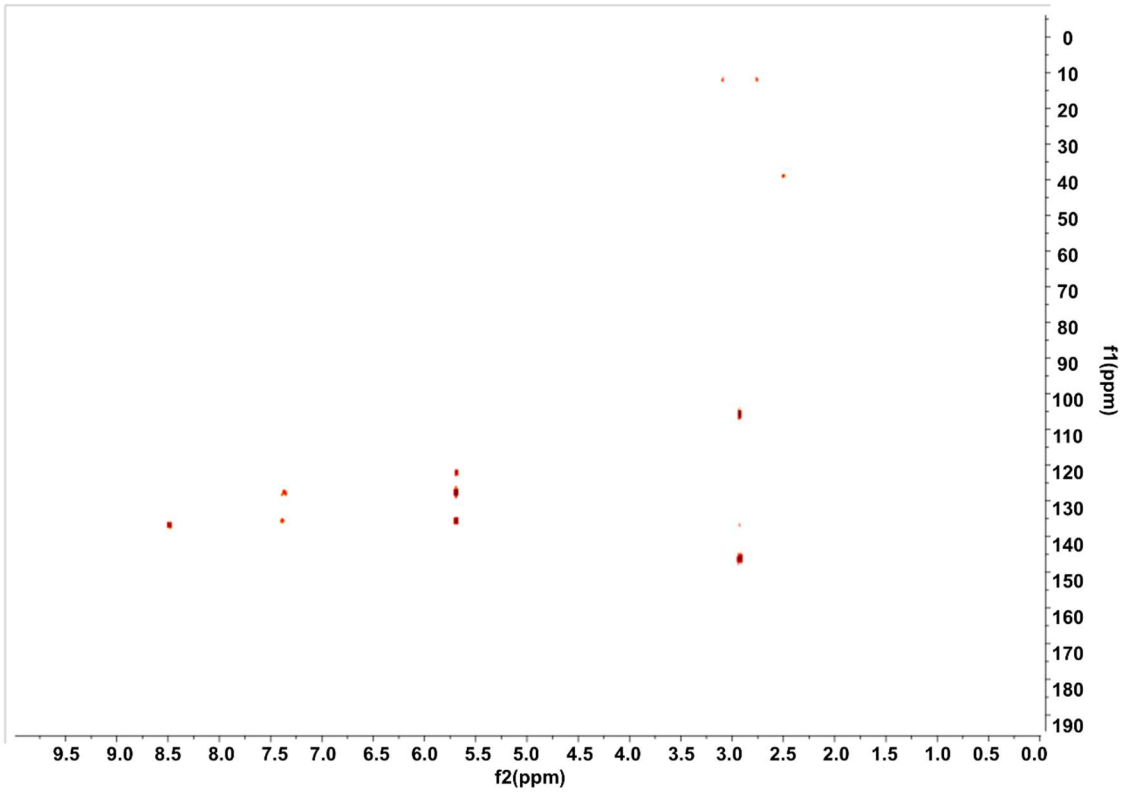

Figure S39. HMBC ^{13}C-^{1}H correlation in DMSO-d_6 solvent of bimane ditriazole **1** at 300 K

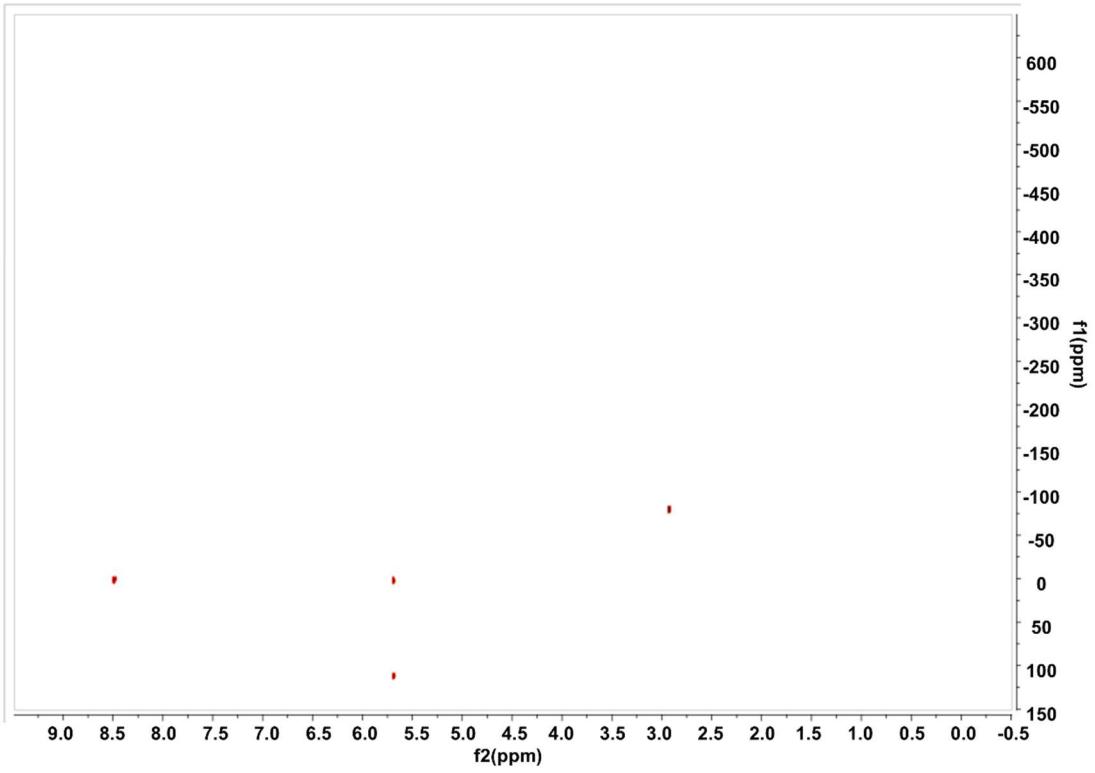

Figure S40. HMBC ^{15}N-^{1}H correlation in DMSO-d_6 solvent of bimane ditriazole **1** at 300 K (standard: nitromethane)

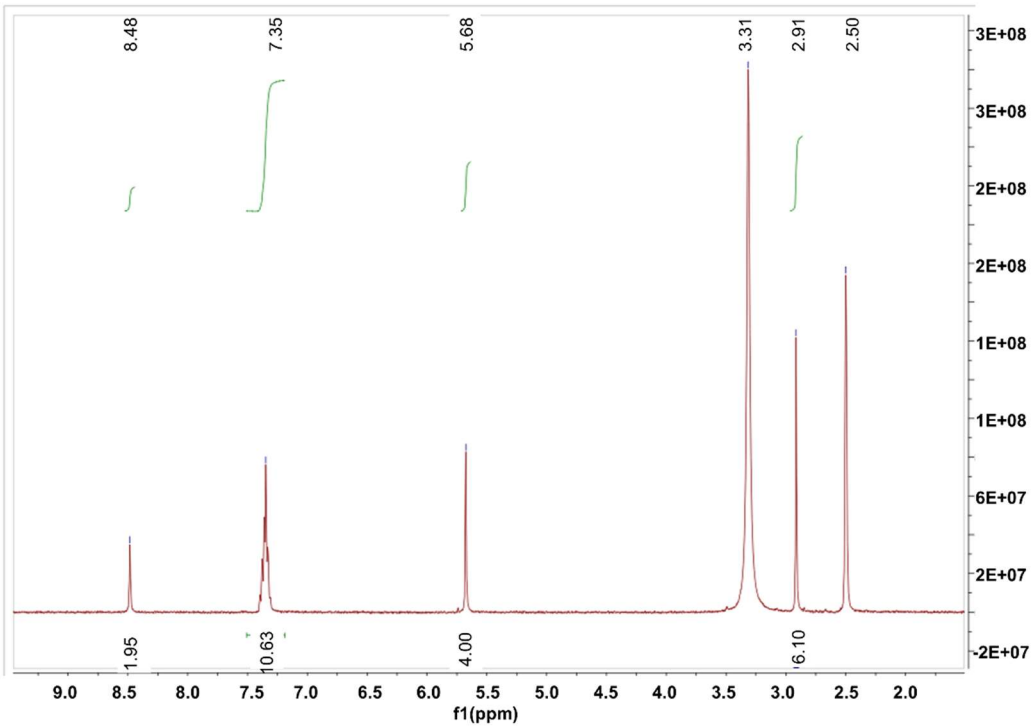

Figure S41. ^{1}H NMR of bimane triazole **1** after addition of 2.5mg Cu(II) in a total of 0.6 mL of DMSO-d_6 solvent at 300 K (no spinning)

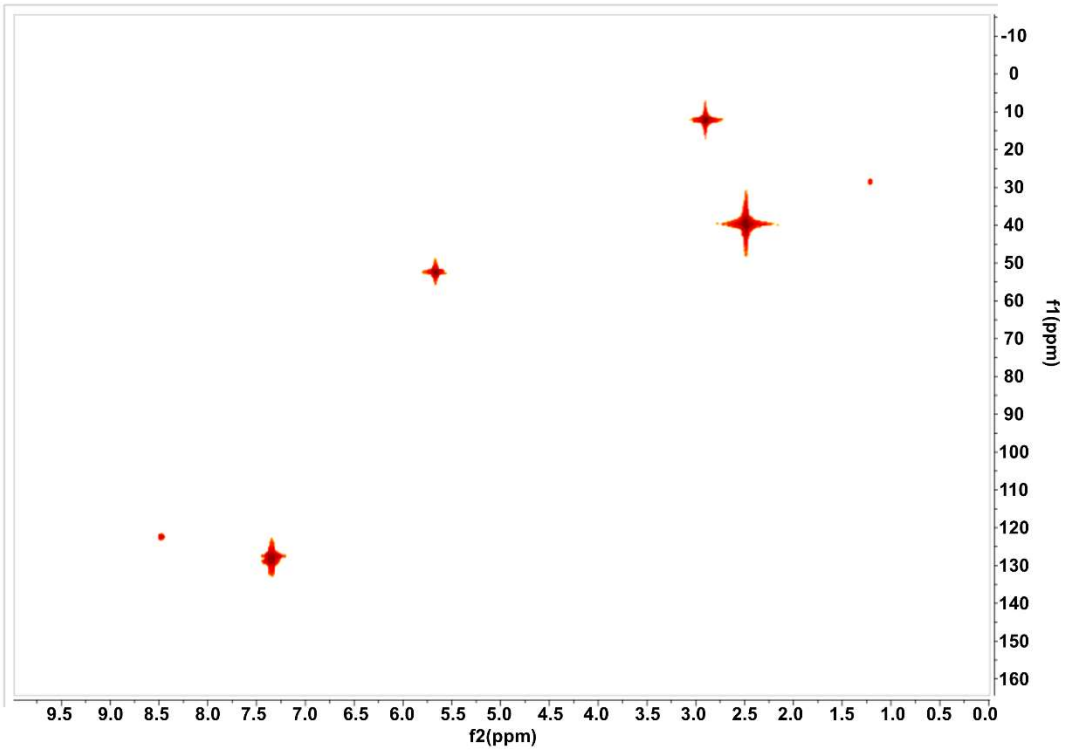

Figure S42. HMQC ^{13}C-^{1}H correlation after addition of 2.5mg Cu(II) in DMSO-d_6 solvent of bimane ditriazole **1** at 300K

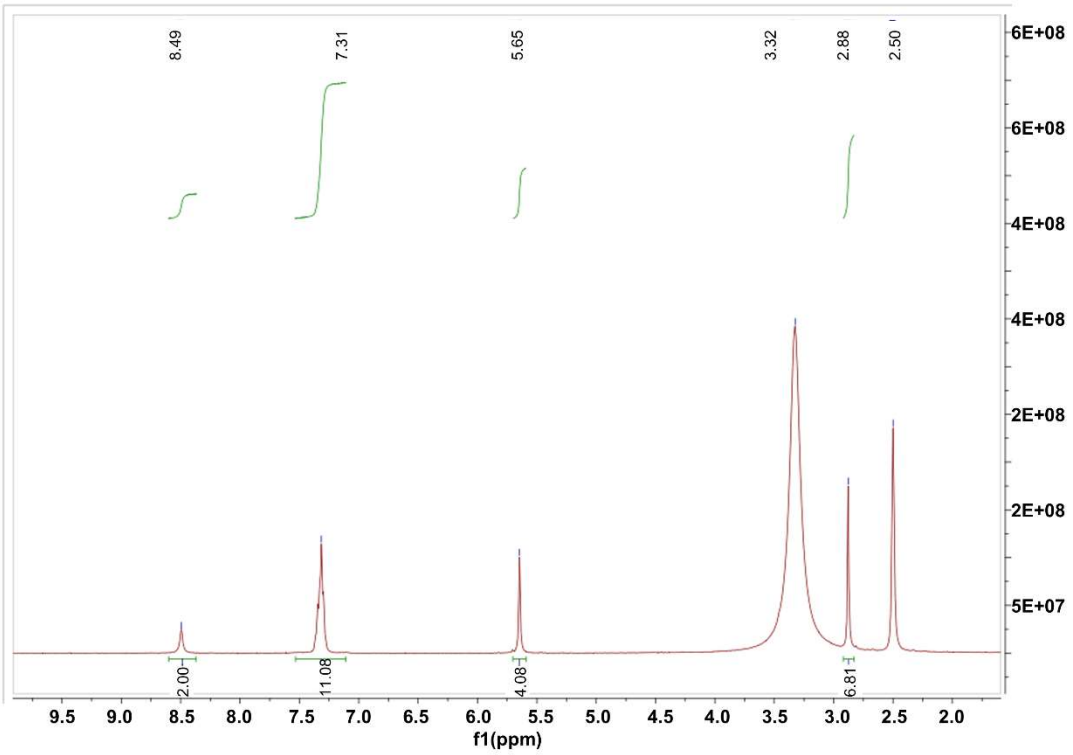

Figure S43. ^{1}H NMR spectra after another addition of 2.5mg Cu(II) (total in 5mg)in DMSO-d_6 solvent of bimane ditriazole **1** at 300K, resulting in the formation of a green solution

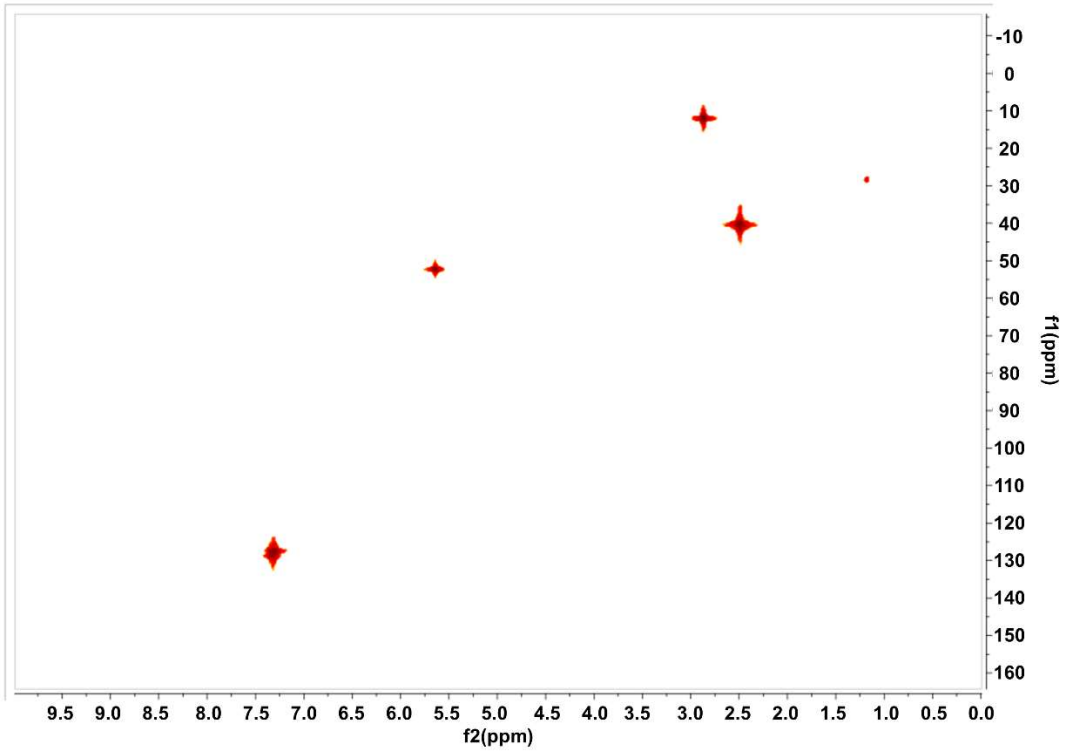

Figure S44. HMQC of ^{13}C-^{1}H NMR correlation spectra after another addition of 2.5mg Cu(II) (total of 5mg) in DMSO-d_6 solvent of bimane ditriazole **1** at 300K

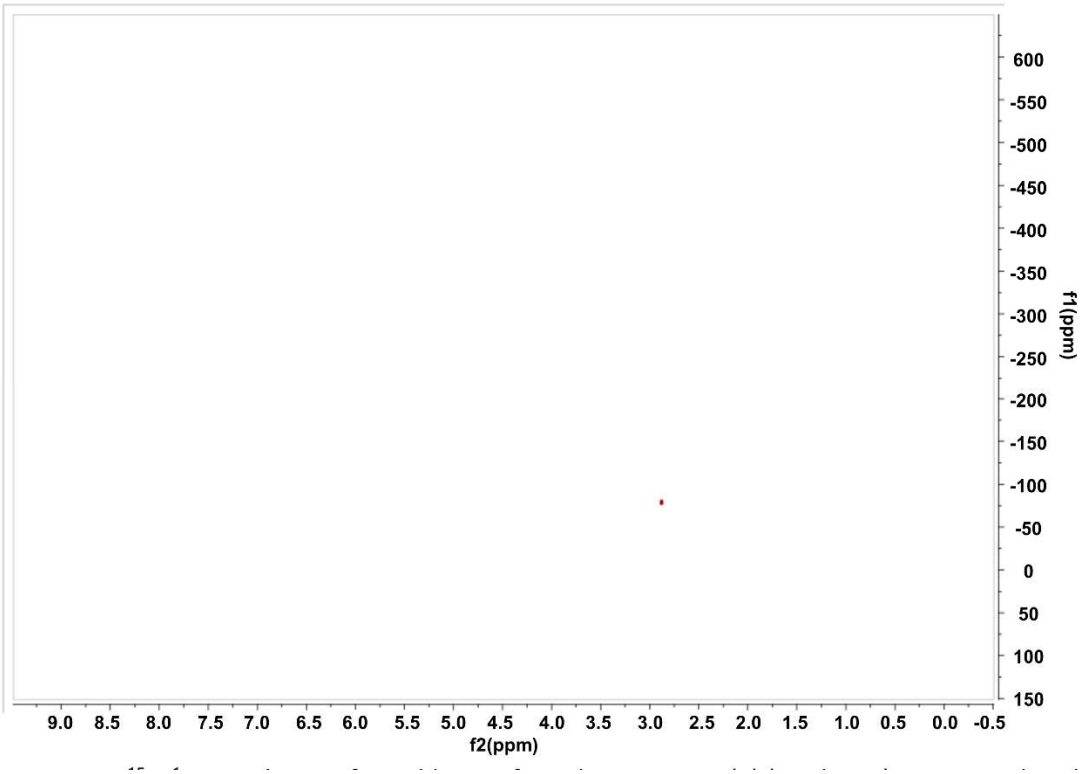

Figure S45. HMBC ^{15}N-^{1}H correlation after addition of another 2.5mg Cu (II) (total 5mg) in DMSO-d_6 solvent of bimane ditriazole **1** at 300K (standard: nitromethane)

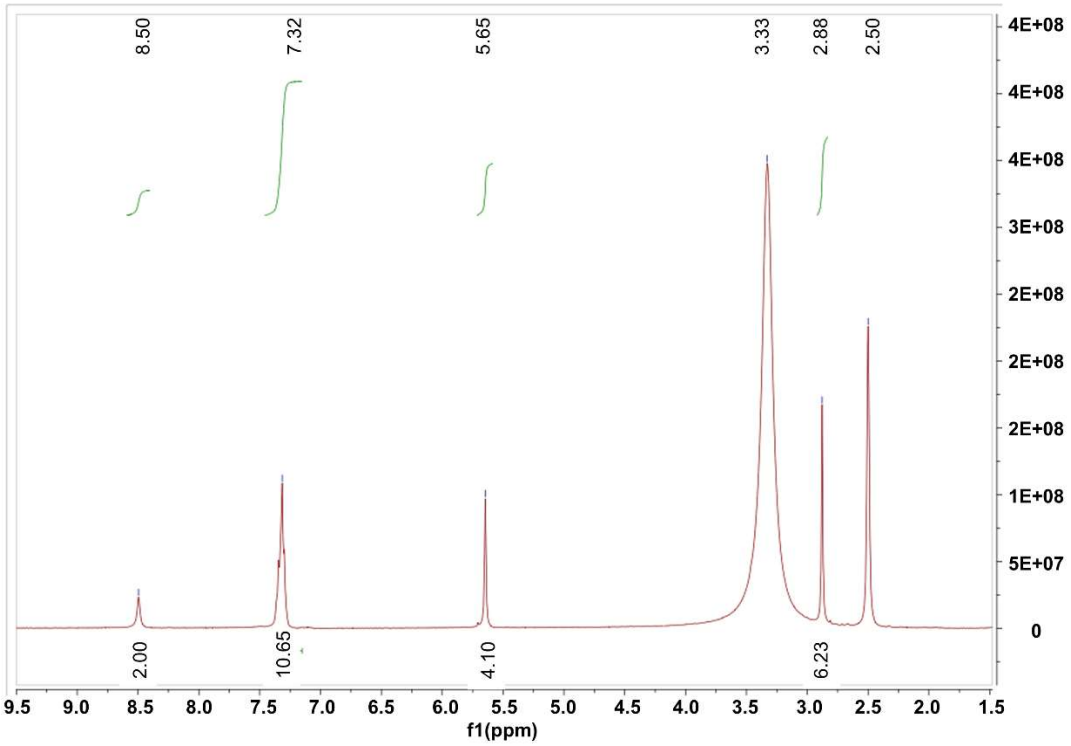

Figure S46. ^{1}H NMR Spectra after another addition of 2.5mg Cu(II) (total in 5mg)in DMSO-d_6 solvent of bimane ditriazole **1** at 300K (after 24 hours)

Summary Figure for FTIR Experiments

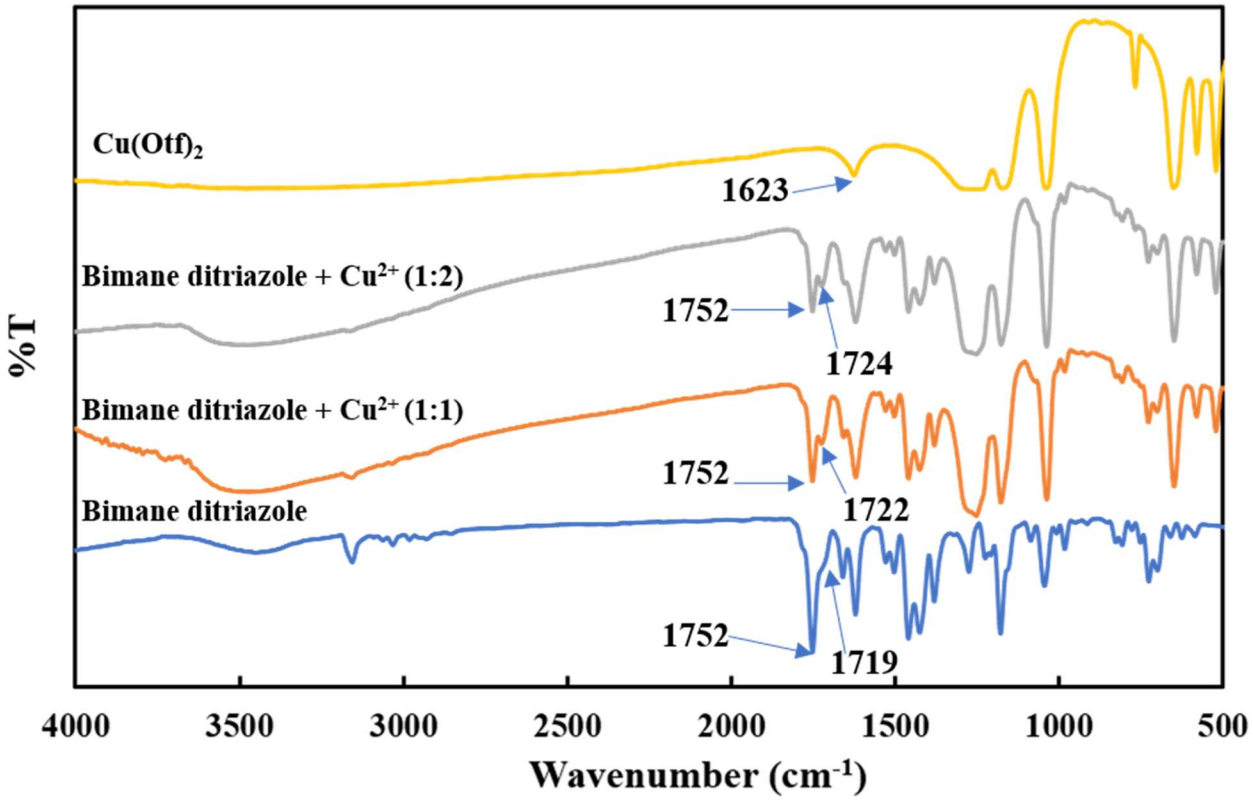

Figure S47. Summary figure of the FTIR spectra of compound **1** (blue line); compound **1** in a 1:1 stoichiometric ratio with copper (II) triflate (orange line); compound **1** in a 1:2 stoichiometric ratio with copper (II) triflate (grey line); and copper (II) triflate (yellow line). The wavenumbers of certain notable peaks are indicated herein.

DESCRIPTION OF ACCOMPANYING VIDEO

The full video was viewed with excitation of the vials at 365 nm using a hand-held, long-wave TLC lamp. Prior to the video, 4 vials were prepared, each of which contains 3 mL of a 25 μM solution of bimane **1** in acetonitrile. The initial additions (between 0.06 minutes and 0.24 minutes) were of 1 mL of a 1 mM copper (II) triflate solution to vials 2, 3, and 4. After that, 100 μL of Milli-Q water was added to vial 2 (between 0.35 and 0.40 minutes), 100 μL of 99.9% methanol was added to vial 3 (between 0.52 and 0.57 minutes), and 100 μL of ethanol (99.5%) was added to vial 4 (between 1.09 and 1.13 minutes).

REFERENCES

[1] Neogi, I.; Das, P. J.; Grynszpan, F. Dihalogen and Solvent-Free Preparation of syn-Bimane. *Synlett* **2018**, *29*, 1043-1046.

[2] Kosower, E. M.; Ben-Shoshan, M. Bimane Acetylenes and Diacetylenes. Bimanes. 33. *J. Org. Chem.* **1996**, *61*, 5871-5884.

[3] Szabo, T.; Benyei, A.; Szilagyi, L. Bivalent Glycoconjugates Based on 1,5-Diazabicyclo[3.3.0]octa-3,6-diene-2,8-dione ("Bimane") as a Central Scaffold. *Carbohydrate Res.* **2019**, *473*, 88-98.

[4] Fu, Y.; Jiang, X.-J.; Zhu, Y.-Y.; Zhou, B.-J.; Zang, S.-Q.; Tang, M.-S.; Zhang, H.-Y.; Mak, T. C. W. A New Fluorescent Probe for Al3+ Based on Rhodamine 6G and its Application to Bioimaging. *Dalton Trans.* **2014**, *43*, 12624-12632.

[5] Pramanik, A.; Abbasi, M.; Maji, K.; Nandi, S. K.; Datta, R.; Haldar, D. Selective Sensing of Ammonium Ion Over Other Biologically Important Ammonia Derivatives by a Coumarin-Based ε-Amino Ester. *ChemistrySelect* **2018**, *3*, 393-398.

[6] Gehlen, M. H. The Centenary of the Stern-Volmer Equation of Fluorescence Quenching: From the Single Line Plot to the SV Quenching Map. *J. Photochem. Photobiol. C* **2020**, *42*, 100338.

[7] Brouwer, A. M.; USE IUPAC Commission Standards for Photoluminescence Quantum Yield Measurements in Solution (IUPAC Technical Report). *Pure Appl. Chem.* **2011**, *83*, 2213-2228.

[8] Gao, F.; Luo, F.; Chen, X.; Yao, W.; Yin, J.; Yao, Z.; Wang, L. Fluorometric Determination of Water in Organic Solvents Using Europium Ion-Based Luminescent Nanospheres. *Microchim. Acta* **2009**, *166*, 163-167.

[9] Song, L.; Wu, Y.-W.; Chai, W.-X.; Tao, Y.-S.; Jiang, C.; Wang, Q.-H. Fluorescence Quenching of a Europium Coordination Compound for the Detection of Trace Amounts of Water: Uncovering the Response Mechanism by Structural Confirmation. *Eur. J. Inorganic Chem.* **2015**, *2015*, 2264-2271.

[10] Kim, Y. H.; Choi, M. G.; Im, H. G.; Ahn, S.; Shim, I. W.; Chang, S.-K. Chromogenic Signalling of Water Content in Organic Solvents by Hydrazone-Acetate Complexes. *Dyes Pigments* **2012**, *92*, 1199-1203.

[11] Niu, C.-G.; Qin, P.-Z.; Zeng, G.-M.; Gui, X.-Q.; Guan, A.-L. Fluorescence Sensor for Water in Organic Solvents Prepared from Covalent Immobilization of 4-Morpholinyl-1,8-Naphthalimide. *Anal. Bioanal. Chem.* **2007**, *387*, 1067-1074.

[12] Niu, C.; Li, L.; Qin, P.; Zeng, G.; Zhang, Y. Determination of Water Content in Organic Solvents by Naphthalimide Derivative Fluorescent Probe. *Anal. Sci.* **2010**, *26*, 671-674.

[13] Li, Z.; Yang, Q.; Chang, R.; Ma, G.; Chen, M.; Zhang, W. N-Heteroaryl-1,8-Naphthalimide Fluorescent Sensor for Water: Molecular Design, Synthesis and Properties. *Dyes Pigments* **2010**, *88*, 307-314.

[14] Kumar, P.; Kaushik, R.; Ghosh, A.; Jose, D. A. Detection of Moisture by Fluorescent OFF-ON Sensor in Organic Solvents and Raw Food Products. *Anal. Chem.* **2016**, *88*, 11314-11318.

[15] Cheng, Wenjing; Xie, Yiting; Yang, Zhiyu; Sun, Yueqing; Zhang, Ming-Zhi; Ding, Yubin; Zhang, Weihua General Strategy for in Situ Generation of a Coumarin-Cu2+ Complex for Fluorescent Water Sensing. *Anal. Chem.* **2019**, *91*, 5817-5823.

[16] Pramanik, A.; Karmakar, J.; Grynszpan, F.; Levine, M. Highly Sensitive Water Detection through Reversible Fluorescence Changes in a syn-Bimane Based Boronic Acid Derivative. *Front. Chem.*, **2021**, *Ahead of Print*; DOI: 10.3389/fchem.2021.782481.